CrystEngComm

PAPER

View Article Online
View Journal | View Issue

Cite this: *CrystEngComm*, 2020, **22**, 3627

Investigating the melting behaviour of polymorphic zeolitic imidazolate frameworks†

Alice M. Bumstead, [a] María Laura Ríos Gómez, [ab] Michael F. Thorne, [a] Adam F. Sapnik,[a] Louis Longley, [a] Joshua M. Tuffnell,[ac] Dean S. Keeble, [d] David A. Keen [e] and Thomas D. Bennett *[a]

Received 17th March 2020,
Accepted 6th May 2020

DOI: 10.1039/d0ce00408a

rsc.li/crystengcomm

Recently, there has been growing interest in the amorphous states of metal–organic frameworks (MOFs). Particular focus has been given to melt-quenched MOF glasses. In this work, to improve our understanding of the factors influencing melting, the thermal response of four closely related zeolitic imidazolate frameworks (ZIFs) was studied. Electron withdrawing ligands were found to lower both the melting and glass transition temperatures, providing a promising strategy for improving the processability of MOFs in the liquid state. Crucially, dense frameworks appear to be essential for melting, with their presence also initiating the melting of open pore frameworks. This opens up the rich polymorphic landscape of ZIFs to the preparation of novel MOF liquids and glasses.

Introduction

The field of metal–organic frameworks (MOFs) has developed considerably in the last 30 years.[1–3] MOFs are composed of metal-containing nodes, known as secondary building units (SBUs), connected by organic linkers.[4] The symmetry and connectivity of the nodes and linkers influence the resulting framework topology.[5,6] The high internal surface area of MOFs along with the potential for open metal sites has prompted research into their potential applications as sorbents, catalysts and biomedical materials.[7–11] Other applications as molecular sensors and redox active materials are also beginning to emerge.[12] Facile solvothermal synthetic methods combined with the large number of metal nodes and organic linkers available has led to the crystal structures of over 80 000 MOFs being deposited in the Cambridge Structural Database.[13]

Recently, there has been growing interest in the physical properties of MOFs, with framework flexibility and defect incorporation being investigated.[14–17] The thermo-mechanical stability of MOFs, and particularly the changes which occur upon exceeding the limits of stability, are also of increasing interest. Pressure or temperature induced solid-state amorphisation, *i.e.* structural collapse without passing through a liquid phase, has been studied in a number of structural families.[18–21] Solid–liquid transitions, or melting, have also been observed in MOFs, though the majority of work centres on one family, known as zeolitic imidazolate frameworks (ZIFs).[17,22,23] Additionally, some 1D and 2D coordination polymers have been reported to melt, particularly by Horike *et al.*[24–28]

ZIFs are composed of divalent transition metal ions connected by imidazolate (Im – $C_3H_3N_2^-$) based linkers; they gain their name from their structural similarity to zeolites.[29–31] First-principles molecular dynamics simulations have demonstrated that melting of ZIFs occurs on a picosecond timescale: rapid de-coordination of an imidazolate linker from a metal ion is followed by dissociation and re-coordination of a new linker in its place.[22,32] The temperature at which the transition to the liquid state is complete is referred to as the melting temperature (T_m). The liquids formed upon heating can then be quenched upon cooling, yielding melt-quenched glasses.[22,23,33] On re-heating, MOF glasses exhibit a glass transition (T_g) to a liquid-like state which is reversible on cooling.[17,23,33] Several MOFs have been reported to retain porosity to gases after melt-quenching and glass formation.[34–37] MOF liquids and glasses are thus an exciting prospect not simply for their novelty but also for their enhanced processability, *i.e.* the feasibility of preparation of

[a] *Department of Materials Science and Metallurgy, University of Cambridge, Cambridge, CB3 0FS, UK. E-mail: tdb35@cam.ac.uk*
[b] *Institute of Materials Research (IIM-UNAM), Circuito Exterior, Ciudad Universitaria, Coyoacán, 04510, D. F., Mexico*
[c] *Cavendish Laboratory, University of Cambridge, Cambridge CB3 0HE, UK*
[d] *Diamond Light Source Ltd, Diamond House, Harwell Campus, Didcot, Oxfordshire, OX11 0DE, UK*
[e] *ISIS Facility, Rutherford Appleton Laboratory, Harwell Campus, Didcot, Oxfordshire, OX11 0QX, UK*

† Electronic supplementary information (ESI) available. CCDC 1990640. For ESI and crystallographic data in CIF or other electronic format see DOI: 10.1039/d0ce00408a

bulk MOF materials, compared to the more ubiquitous crystalline powders.[22,36]

The first example of a melting MOF was ZIF-4 [$Zn(Im)_2$], which crystallises in an orthorhombic *Pbca* space group with the **cag** topology.[29,33] It undergoes thermal amorphisation on heating above 300 °C before recrystallising to a more dense polymorph with the $I4_1cd$ space group and the **zni** topology above 400 °C.[33,38,39] This polymorph then melts at T_m = 593 °C.[33,38,39]

A number of mixed linker ZIFs also melt and form glasses (Table 1). Of these materials, ZIF-62 and TIF-4 crystallise in an orthorhombic *Pbca* space group with the **cag** topology (TIF – tetrahedral imidazolate framework).[29,30,40] However, both forms of ZIF-76 have a cubic crystal structure with the $P\bar{4}3m$ space group and the LTA topology.[23,37] Interestingly, another open, cubic framework, ZIF-8 [$Zn(mIm)_2$] (mIm – 2-methylimidazolate – $C_4H_5N_2^-$), decomposes prior to melting.[22,32,33] Theoretical calculations performed by Gaillac *et al.* demonstrated ZIF-8 melts significantly above its experimental decomposition temperature.[32,41] This is attributed to the relatively high barrier to linker diffusion between zinc tetrahedra due to the open network structure.[22,32,33] It was concluded that dispersion interactions from the framework stabilise the uncoordinated linkers as they move to new metal sites during melting.[32] Consequently, denser frameworks will have more dispersion interactions stabilising the linker and hence present a lower energy barrier to dissociation.[32] It is clear, therefore, that framework topology and density are important factors influencing melting.

The metal centre present within a ZIF can also alter its melting behaviour. For example, a cobalt-containing analogue of ZIF-62 [$Co(Im)_{1.65}(bIm)_{0.35}$] (bIm – benzimidazolate – $C_7H_5N_2^-$) melts at a lower temperature (432 °C) than the zinc-containing material [$Zn(Im)_{1.75}(bIm)_{0.25}$] (437 °C).[34] However, the different stoichiometry of these two ZIFs may influence their thermal response. For example, it has recently been demonstrated that for mixed linker ZIFs composed of Im and a bulkier linker such as bIm, reducing the concentration of bIm in the framework can reduce the melting point of the ZIF significantly (Table 1).[35] However, the complete absence of the bulky bIm linker leads to the formation of ZIF-4 and a rise in the melting temperature due to recrystallisation to the **zni** topology prior to melting.[33] Further studies on mixed linker ZIFs demonstrated that the presence of a third ligand also lowers the melting point by introducing more disorder in the crystal structure.[42] These examples highlight the importance of framework chemistry on melting.

In order to expand the number of MOFs that melt prior to decomposition and find novel MOF glasses with interesting properties, the melting process must first be understood in greater depth. However, it is still unclear how factors such as crystal structure and chemistry can be used to control melting. To investigate this, four closely related ZIFs were studied: TIF-4 [$Zn(Im)_{1.8}(mbIm)_{0.2}$], ZIF-UC-5 [$Zn(Im)_{1.8}(ClbIm)_{0.2}$], ZIF-76-mbIm [Zn(Im)(mbIm)] and ZIF-76 [Zn(Im)(ClbIm)] (Fig. 1, Table 2) (ClbIm – 5-chlorobenzimidazolate – $C_7H_4N_2Cl^-$, mbIm – 5-methylbenzimidazolate – $C_8H_7N_2^-$). These names are those reported in the literature, though the chemical compositions reported here are different due to the different synthetic methods used.[23,30,37,40,43] The selection of these four materials allows the effect of both linker chemistry and crystal structure upon melting to be studied. For example, TIF-4 and ZIF-UC-5 contain different substituted benzimidazolate linkers: mbIm and ClbIm. However, they both crystallise in an orthorhombic *Pbca* space group and have the **cag** topology. In addition, TIF-4 and ZIF-76-mbIm both contain tetrahedral zinc SBUs and Im and mbIm organic linkers. However, TIF-4 crystallises in an orthorhombic *Pbca* space group with the **cag** topology whilst ZIF-76-mbIm crystallises in a cubic $P\bar{4}3m$ space group with the LTA topology.

Experimental

Materials

Imidazole (99.5%), 5-chlorobenzimidazole (96%) and D_2O (20% DCl) were purchased from Sigma Aldrich. Dimethyl sulfoxide (DMSO)-d_6 (99.8 atom% D, contains 0.03% (v/v) tetramethylsilane (TMS)) was purchased from VWR. Zinc nitrate hexahydrate (98%) and 5-methylbenzimidazole (98%) were purchased from Alfa Aesar. *N*,*N*-Dimethylformamide (DMF) (99.5%) and sodium hydroxide pellets were purchased from Fischer Scientific. *N*,*N*-Diethylformamide (DEF) (99%) and dichloromethane (DCM) (99.9% stabilised with amylene) were purchased from Acros Organics. All materials were used without further purification.

Table 1 Examples of ZIFs reported to melt. All values reported here are under ambient pressure. Raised pressures have been demonstrated to lower the melting point.[47,48] ZIF-62 (Zn) and ZIF-62 (Co) have been reported with a range of compositions so exhibit a range of melting temperatures and glass transition temperatures

MOF	Formula	Space group	T_m (°C)	T_g (°C)	Ref
ZIF-4	$Zn(Im)_2$	*Pbca*	593	292	23, 33, 38, 49
ZIF-62 (Zn)	$Zn(Im)_{2-x}(bIm)_x$ (x = 0.05–0.35)	*Pbca*	372–441	298–320	23, 34, 35, 49, 50
ZIF-62 (Co)	$Co(Im)_{2-x}(bIm)_x$ (x = 0.10–0.30)	*Pbca*	386–432	260–290	23, 34, 35, 49, 50
ZIF-76 isomorphs	$Zn(Im)_{1.62}(ClbIm)_{0.38}$	$P\bar{4}3m$	451	310	37, 49
	$Zn(Im)_{1.33}(mbIm)_{0.67}$	$P\bar{4}3m$	471	317	37, 49
TIF-4	$Zn(Im)_{1.5}(mbIm)_{0.5}$	*Pbca*	467	343	23

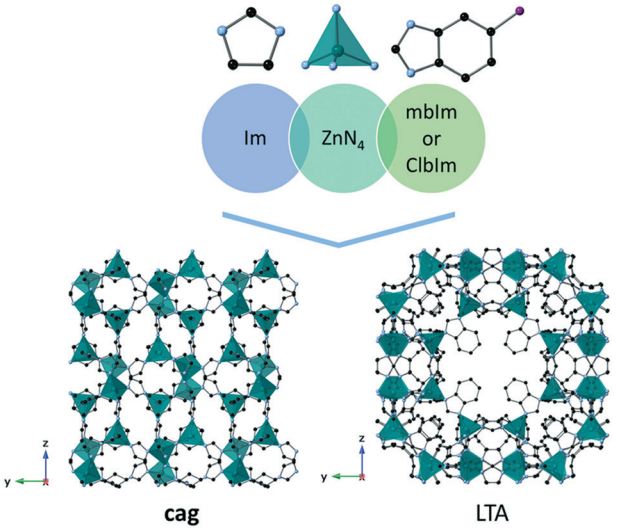

Fig. 1 Comparison of the **cag** (TIF-4 and ZIF-UC-5) and LTA (ZIF-76-mbIm and ZIF-76) frameworks and the components of both: Im, ZnN_4 tetrahedra and either mbIm or ClbIm. Atoms shown: carbon (black), nitrogen (blue), zinc (green) and linker substituent (purple). Hydrogens omitted from all structures for clarity. Linker substituent omitted from LTA framework for clarity. Adapted from originally reported CIF files.[30,40]

Table 2 Four ZIF systems studied in this work

MOF	Formula	Space group	Topology
TIF-4	$[Zn(Im)_{1.8}(mbIm)_{0.2}]$	*Pbca*	**cag**
ZIF-UC-5	$[Zn(Im)_{1.8}(ClbIm)_{0.2}]$	*Pbca*	**cag**
ZIF-76-mbIm	[Zn(Im)(mbIm)]	$P\bar{4}3m$	LTA
ZIF-76	[Zn(Im)(ClbIm)]	$P\bar{4}3m$	LTA

Characterisation techniques

Single crystal X-ray diffraction (SCXRD). Single crystal X-ray diffraction data on a ZIF-76-mbIm crystal were collected on an Oxford Diffraction Gemini E Ultra single crystal diffractometer equipped with an Atlas CCD area detector. Cu K_α (λ = 1.54184 Å) radiation was used. The experiment was performed at 298 K on a single crystal (0.25 × 0.20 × 0.18 mm) with a collection time of 2 hours to achieve completeness. Structure solution was performed using SUPERFLIP (a charge-flipping based program) and the refinement was performed using SHELXL both in the WinGX suite version 2018.2.[44–46] See ESI† for full refinement details.

Powder X-ray diffraction (PXRD). Data were collected on a Bruker D8 ADVANCE diffractometer equipped with a position sensitive LynxEye detector. Cu K_α (λ = 1.54184 Å) radiation was used. The samples were compacted into 5 mm disks and rotated during data collection in the 2θ range of 5–40° at ambient temperature. Pawley refinements were performed using TOPAS-Academic Version 6.[51] Thompson–Cox–Hastings pseudo-Voigt (TCHZ) peaks shapes were used along with a simple axial divergence correction. The lattice parameters were refined against reported values for the structure in the 2θ range of 5–40°. The zero point error was also refined.

Differential scanning calorimetry (DSC). Data were collected on a Netzsch DSC 214 Polyma Instrument. Heating and cooling rates of 10 °C min^{-1} were used in conjunction with a flowing argon atmosphere. Sealed aluminium pans (30 μL) were used with a hole punctured in the lid to prevent pressure build-up. An empty aluminium pan was used as a reference. Background corrections were performed using the same heating cycle on an empty aluminium crucible. The melting temperature (T_m) was taken as the offset (the end point) of the melting endotherm. The glass transition temperature (T_g) was taken as the mid-point of the change in gradient of the heat flow of the DSC on the 2nd upscan. This marks where the glass changes from a rigid to a more flexible state.

Thermogravimetric analysis (TGA). Data were collected on a TA Instruments SDT-Q600 using alumina pans (90 μL). Heating rates of 10 °C min^{-1} were used along with a flowing argon atmosphere.

^{1}H nuclear magnetic resonance (NMR) spectroscopy. ^{1}H NMR spectra were recorded at 298 K using a Bruker AVIII 500 MHz Spectrometer with a dual $^{13}C/^1H$ (DCH) cryoprobe at the Department of Chemistry, University of Cambridge. All samples were dissolved in a mixture of DCl (20%)/D_2O and DMSO-d_6 in a 1 : 5 ratio. Tetramethylsilane (TMS) was used as a reference. All data processing was performed using TopSpin 4.0.7.[52]

Variable temperature pair distribution function (PDF). X-ray total scattering data were collected at beamline I15-1, Diamond Light Source, UK (EE20038-2). All samples were ground and sealed in quartz capillaries (1.30 mm inner diameter). Data were collected for the background, empty capillary and for all samples to a Q_{max} of 26.0 $Å^{-1}$ (λ = 0.161669 Å, 76.69 keV). Data were collected at 25, 100, 200, 300, 400, 430, 450, 460 and 25 °C for ZIF-76-mbIm with 10% flux to minimise sample damage. Data were collected at 25, 100, 200, 300, 400, 420, 440 and 25 °C for TIF-4 with 100% flux. Data were processed in a Q range of 0.55–19.0 $Å^{-1}$ for ZIF-76-mbIm and a Q range of 0.50–26.0 for TIF-4. Data correction and subsequent Fourier transform was performed using the GudrunX program to obtain the PDF for each sample at each temperature.[53,54]

Synthetic methods

Synthesis of TIF-4 and ZIF-UC-5. Zinc nitrate hexahydrate (0.38 g, 1.28 mmol), imidazole (1.84 g, 27.0 mmol) and either 5-methylbenzimidazole (0.396 g, 3.00 mmol) or 5-chlorobenzimidazole (0.458 g, 3.00 mmol) were dissolved in *N*,*N*-dimethylformamide (DMF) (18.8 ml) and heated at 130 °C for 48 hours. The polycrystalline powder was isolated by vacuum filtration and washed with fresh DMF. The sample was then soaked in dichloromethane (DCM) (3 ml) for 24 hours. Excess DCM was decanted and the sample was activated by heating under vacuum at 100 °C for 3 hours.

This was based on reported syntheses of TIF-4 and ZIF-62.[30,40,47]

Optimisation of ZIF-76-mbIm synthesis. Imidazole and 5-methylbenzimidazole were dissolved in a mixture of DMF (5.75 ml) and *N*,*N*-diethylformamide (DEF) (5.75 ml). Zinc nitrate hexahydrate (0.26 g, 0.87 mmol) and sodium hydroxide solution (2.5 mol dm^{-3}) were added and the solution was heated at 90 °C for 120 hours (Table S1†). The polycrystalline powder was collected by vacuum filtration and washed with fresh DMF. The sample was then soaked in DCM (3 ml) for 24 hours. Excess DCM was decanted and the sample was activated by heating under vacuum at 100 °C for 3 hours. This was based on reported methods for the synthesis of ZIF-76 and ZIF-76-mbIm.[30,37,55]

Synthesis of phase pure ZIF-76-mbIm and ZIF-76. Imidazole (0.12 g, 1.76 mmol) and either 5-methylbenzimidazole (0.11 g, 0.83 mmol) or 5-chlorobenzimidazole (0.13 g, 0.85 mmol) were dissolved in a mixture of DMF (5.75 ml) and DEF (5.75 ml). Zinc nitrate hexahydrate (0.26 g, 0.87 mmol) and sodium hydroxide solution (2.5 mol dm^{-3}, 0.26 ml, 0.65 mmol) were added and the solution was heated at 90 °C for 120 hours. The polycrystalline powder was recovered by vacuum filtration and washed with fresh DMF. The sample was then soaked in DCM (3 ml) for 24 hours. Excess DCM was decanted and the sample was activated by heating under vacuum at 100 °C for 3 hours. Based on previously reported methods.[30,37,55]

Results and discussion

Effect of organic linker chemistry on thermal behaviour

TIF-4 and ZIF-UC-5 were studied in order to distinguish between the effects of linker chemistry and framework topology. TIF-4 $[Zn(Im)_{1.5}(mbIm)_{0.5}]$ melts at 467 °C whilst ZIF-UC-5 $[Zn(Im)_{1.63}(ClbIm)_{0.37}]$ melts at the lower temperature of 432 °C.[23,40,43] However, it is unclear whether this difference is caused by the different linker chemistry or by the different stoichiometry of the two materials. To address this, TIF-4 and ZIF-UC-5 were prepared by a modification of the originally reported synthesis, avoiding the use of benzene as a structure directing agent.[40,43] A microcrystalline powder was obtained in both cases. Both crystallise in an orthorhombic *Pbca* space group. Phase purity and crystallinity were confirmed by powder X-ray diffraction (PXRD) (Fig. S1 and S2, Tables S2 and S3†). The ratio of imidazolate to substituted benzimidazolate $[Zn(Im)_{1.8}(XbIm)_{0.2}]$ for our samples was confirmed by ^{1}H NMR spectroscopy (Fig. S3 and S4†), a ratio that is different to those in the original reports.[40,43] The synthetic method used here was based on one used for ZIF-62, which yielded particle sizes of *ca.* 10 μm.[47] Additionally, the maximum particle size of ZIF-UC-5 was found previously to be 50 μm.[43] Significantly larger particles were not observed here. Previous calculations have demonstrated that a methyl group has a larger van der Waals volume (13.67 cm^3 mol^{-1}) than a chlorine atom (12.0 cm^3 mol^{-1}) and hence that 5-methylbenzimidazolate has a marginally larger van der Waals volume (121.5 cm^3 mol^{-1}) than 5-chlorobenzimidazolate (119.0 cm^3 mol^{-1}).[56,57] However, chlorine is electron withdrawing whilst a methyl group is electron donating. So, both steric and electronic effects are likely to affect melting behaviour.

The thermal response of both TIF-4 and ZIF-UC-5 was investigated by differential scanning calorimetry (DSC) and thermogravimetric analysis (TGA) (Fig. 2 and S5–S10†). TGA showed that significant mass loss for both samples occurred above 575 °C suggesting that decomposition began above this temperature (Fig. S5 and S6†). Both structures exhibited broad endothermic features in the DSC in the range from 150–250 °C that were associated with desolvation due to residual solvent left in the pores after activation. They also exhibited a clear endotherm coupled with a minimal loss in mass: a characteristic feature of melting. The melting temperature for TIF-4 was found at 440 °C whilst that of ZIF-UC-5 was found at 428 °C (Fig. 2 and S7 and S8,† Table 3). After heating above the melting offset, the samples were cooled back to room temperature and then re-heated to 400 °C. This yielded glass transition temperatures of 350 and 336 °C for a_gTIF-4 and a_gZIF-UC-5 respectively (Fig. 2, Table 3, Fig. S9 and S10†). Subsequent PXRD confirmed both samples were amorphous (Fig. S11†) and ^{1}H NMR spectroscopy confirmed both glasses had a ratio of Im to XbIm near identical to the crystalline frameworks (S12 and S13†). These are denoted a_gTIF-4 and a_gZIF-UC-5 in keeping with previous nomenclature.[23,43,58]

The lower melting offset of ZIF-UC-5 compared to TIF-4 is attributed to two factors: i) the electron withdrawing chlorine substituent weakening the Zn–N coordination bond, and ii) the smaller van der Waals volume of ClbIm causing a reduction in steric hindrance around the metal centre and therefore facilitating linker dissociation during melting (as suggested by

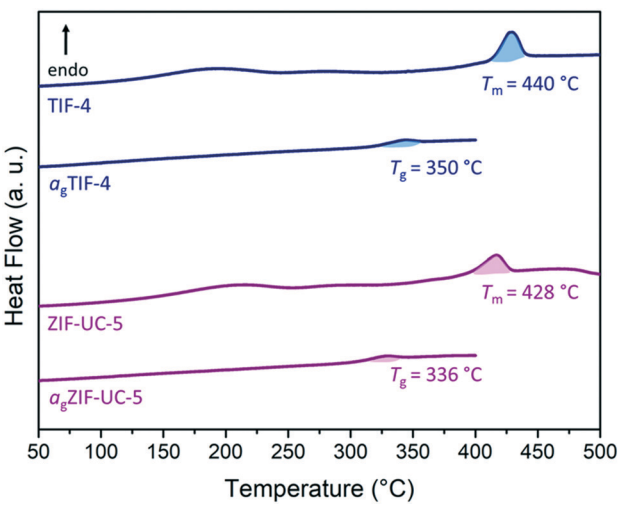

Fig. 2 DSC traces of structural isomorphs: TIF-4 (blue) and ZIF-UC-5 (pink). Heat flow traces stacked by *y* offset. Features of interest, *i.e.* T_m and T_g, are highlighted in the figure as a guide. The melting temperature (T_m) was taken as the offset of the melting endotherm. The glass transition temperature (T_g) was taken as the mid-point of the change in gradient of the heat flow of the DSC on the 2nd upscan.

Table 3 Summary of thermal data for TIF-4 and ZIF-UC-5 in this work

Sample	Composition	T_m (°C)	T_g (°C)
TIF-4	$Zn(Im)_{1.8}(mbIm)_{0.2}$	440	350
ZIF-UC-5	$Zn(Im)_{1.8}(ClbIm)_{0.2}$	428	336

Henke *et al.*[35]). Previous studies on halogenated systems have demonstrated the influence of the electron withdrawing effect.[37,43] For example, replacing 5-chlorobenzimidazolate in ZIF-UC-5 with 5-fluorobenzimidazolate was previously shown to lower the melting temperature by 11 °C, with this effect attributed to the stronger electron withdrawing nature of the fluorinated linker.[43] This was supported by density functional theory calculations, highlighting a reduction in the average Zn–N bond energy by 2.88 kJ mol^{-1} in the fluorinated ZIF.[43] However, a reduction in steric hindrance at the tetrahedral metal site has also been demonstrated to lower the melting temperature, by facilitating linker dissociation.[35] It is therefore likely that both steric and electronic factors have a degree of control over this process with both favouring a reduction in T_m.

One possible strategy to deconvolute these two effects would be the use of a sterically bulky but strongly electron withdrawing linker such as 5-(trifluoromethyl)benzimidazole in the synthesis of a ZIF. The formation, and subsequent measurement of the thermal response of this as-yet-unknown ZIF would determine whether the steric hindrance at the tetrahedral metal centre, or, the weakening of the Zn–N coordination bond is the dominant factor controlling melting. This is a highly promising avenue for future work.

The lower glass transition temperature of ZIF-UC-5 than TIF-4 was ascribed to the smaller van der Waals volume of chlorine compared to the methyl group.[37,56,57] Hence, the dispersion forces in TIF-4 are stronger and more energy is required for the methyl groups to move past one another and for the glass to transition to a more liquid-like, mobile state.[32,37] The particle size of these ZIFs may affect their ability to conduct heat and hence the temperature at which they undergo the glass transition. However, crystalline particle size alters significantly on transition to the liquid state, with the coalescence of many particles being a common observation.[37] As such, it was not possible to infer the influence of particle size on the glass transition here. Overall, the results presented here suggest that the use of halogenated linkers may provide a promising strategy for lowering the melting and glass transition temperatures of MOFs.

The melting offset of TIF-4 $[Zn(Im)_{1.8}(mbIm)_{0.2}]$ (440 °C) in this work is lower than that previously reported for TIF-4 $[Zn(Im)_{1.5}(mbIm)_{0.5}]$ (467 °C).[23] Additionally, the melting offset of ZIF-UC-5 $[Zn(Im)_{1.8}(ClbIm)_{0.2}]$ (428 °C) observed here is lower than the offset previously observed for ZIF-UC-5 $[Zn(Im)_{1.63}(ClbIm)_{0.37}]$ (*ca.* 462 °C).[43] Henke *et al.* recently found the same phenomenon in a series of ZIF-62 MOFs of varying composition $[Zn(Im)_{2-x}(bIm)_x]$: reducing the content of bIm reduced the melting temperature of ZIF-62 by as much as 60 °C.[35] This was rationalised by the smaller steric hindrance of the zinc tetrahedra when less benzimidazolate was present in the framework, thus assisting the dissociation and re-association of imidazolate linkers during melting.[35] The results obtained here support their work and suggest that lowering the content of the more sterically bulky linker in mixed linker MOFs is a promising strategy for lowering the melting temperature.

To investigate the thermal response of TIF-4 $[Zn(Im)_{1.8}(mbIm)_{0.2}]$ further, variable temperature total scattering data were collected at beamline I15-1 at the Diamond Light Source (Fig. 3 and S14†). TIF-4 $[Zn(Im)_{1.8}(mbIm)_{0.2}]$ was heated to 440 °C, *i.e.* beyond the offset of melting. Data were collected at *ca.* 100 °C intervals to 400 °C, then at 420 °C and 440 °C. Measurements were also taken before and after heating to allow comparison between the crystalline sample and the glass. Fourier transformation of the corrected total scattering data gave the pair distribution function $G(r)$. Here we make use of the $D(r)$ form to accentuate the high r correlations (Fig. 3).

The short-range order was maintained throughout heating with the first five correlations corresponding to C=C/C–N, Zn–N, Zn–C, Zn–N and Zn–Zn (Fig. 3). These are the expected short-range order correlations found for most ZIFs, suggesting that the sample has not decomposed on heating or exposure to the beam.[59] However, the long-range order was lost at 400 °C as no clear high r correlations ($r > 8.0$ Å) are visible above this temperature. This is just below the onset of melting in the DSC trace. We ascribe the lower onset of melting in the PDF either to the presence of synchrotron radiation, or to the non-linear heating profile with multiple isothermal segments used to collect the total scattering data compared to the DSC data.

No substantial changes in the $D(r)$ after liquid formation were observed, suggesting that the time spent in the liquid state has minimal influence on the resulting glass structure.

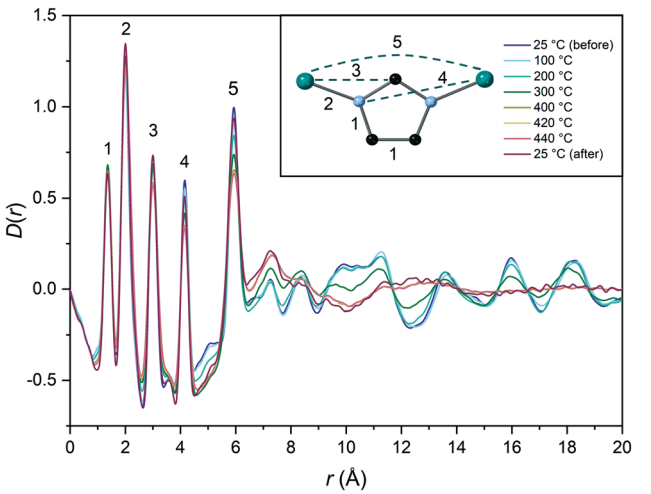

Fig. 3 Pair distribution function, $D(r)$, of TIF-4 at 25, 100, 200, 300, 400, 420, 440 and 25 °C. Inset shows an imidazolate ion coordinated to two zinc ions. The first five correlations are shown on this diagram. Atoms shown: carbon (black), nitrogen (blue), zinc (green).

Whilst some broadening is observed due to increased thermal motion, the recovery upon cooling suggests chemical connectivity is largely retained on glass formation and that thermal disorder in the crystalline and glass state are similar. Together, these results support melting and glass formation of TIF-4.

Optimisation of ZIF-76-mbIm synthesis

To investigate how crystal structure influences melting, TIF-4 was then compared to ZIF-76-mbIm, a structural polymorph, previously reported to melt at 471 °C of composition $[Zn(Im)_{1.33}(mbIm)_{0.67}]$.[37] The synthesis in the original report of ZIF-76 only gave quantities sufficient for single crystal X-ray diffraction.[30] Subsequent efforts then concentrated on increasing the product yield through addition of NaOH, resulting in various chemical compositions reported for the bulk products.[37,55]

Replication of the synthesis reported by Zhou *et al.* using 1.30 mmol of NaOH led to a mixed phase product (Fig. 4 and S15 and S16, Tables S4 and S5†) with additional peaks visible in the diffraction pattern (marked by asterisks).[37] This mixed phase material had a formula unit of $[Zn(Im)_{1.4}(mbIm)_{0.6}]$ determined by ^{1}H NMR spectroscopy (Fig. S17†). These additional peaks were found to index to the crystal structure of TIF-4. Peralta *et al.* reported that too much NaOH led to a mixed phase product.[55] The volume of NaOH in the synthetic route to ZIF-76-mbIm was therefore varied (Fig. 4 and S18–S22, Tables S6–S9†). Reducing the volume of NaOH increased the purity of the product and omitting NaOH from the synthesis gave single crystals with a 6% yield and a particle size of *ca.* 500 μm (Fig. S23†). This particle size agreed with previous reports that obtained single crystal samples.[30,55] This single crystal sample was found to have a formula unit of $[Zn(Im)_{0.9}(mbIm)_{1.1}]$ by ^{1}H NMR spectroscopy (Fig. S19†). Notably, the single crystal material had a considerably higher content of mbIm in its formula unit than the mixed phase material. Halving the molar volume of base added, *i.e.* 0.65 mmol NaOH, yielded ZIF-76-mbIm as a microcrystalline phase pure product with a yield of 67% (Table S1†). Previous reports of bulk ZIF-76 reported particle sizes of less than 10 μm.[55] To confirm the structure reported previously for ZIF-76,[30] a single crystal of ZIF-76-mbIm was selected and the structure solved by single crystal X-ray diffraction in the cubic $P\bar{4}3m$ space group (a = 22.6840(6) Å, V = 11 672.4(9) Å^3, Table S10†).

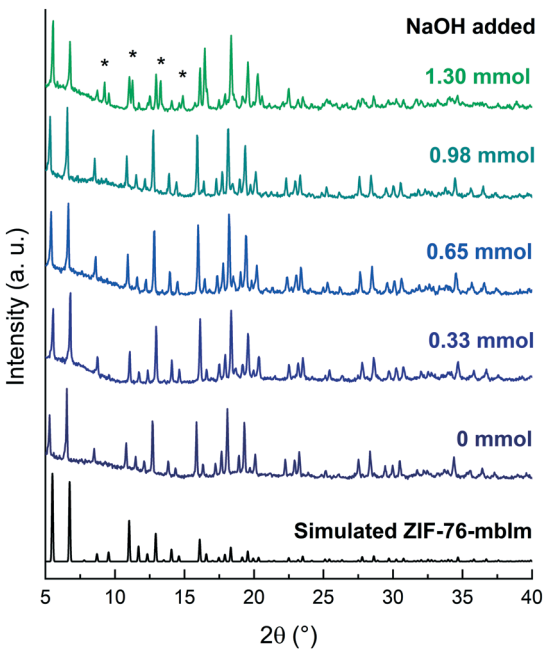

Fig. 4 Powder X-ray diffraction patterns of ZIF-76-mbIm with varying NaOH in the synthesis. Reduction of the number of moles of base used in the synthesis from 1.30 mmol (light green) to 0 mmol (dark blue) systematically improved the purity of the product with 0.65 mmol providing the best combination of purity and yield. Asterisks used to highlight additional peaks in the diffraction pattern.

One possible explanation for the appearance of the TIF-4 phase with increasing volumes of NaOH may be the change in pH of the reaction mixture. Imidazole possesses a higher pK_a (14.4) than benzimidazole type ligands (12.75).[60] Increasing the pH of the solution through NaOH addition therefore results in the deprotonation of more imidazole, and facilitates inclusion within the MOF structure. This would hence favour the formation of TIF-4 as it has a higher content of imidazole in the formula unit.

The formula of ZIF-76-mbIm was found by ^{1}H NMR spectroscopy to be [Zn(Im)(mbIm)] compared to that of $[Zn(Im)_{1.8}(mbIm)_{0.2}]$ for TIF-4 (Fig. S24†). Efforts were made to investigate the effect of increasing the ratio of Im : mbIm to provide a system of $[Zn(Im)_{1.8}(mbIm)_{0.2}]$ composition crystallising in the LTA topology, which could be compared to the identical composition with the **cag** topology, *i.e.* TIF-4.

Increasing the Im : mbIm ratio led to immediate formation of TIF-4 as an impurity, whilst further increases resulted in the formation of TIF-4 as the only product (Fig. 5 and S25–S36,† Tables S11–S16†). This was accompanied by a sequential decrease in the content of mbIm in the formula unit from [Zn(Im)(mbIm)] for an input ratio of 2.0 : 1 Im : mbIm to $[Zn(Im)_{1.7}(mbIm)_{0.3}]$ for an input ratio of 5.0 : 1. We rationalise this through consideration of the relative linker ratios in ZIF-76-mbIm and TIF-4, their relative energies and the symmetry constraints of the *Pbca* space group. To the best of our knowledge, no report has calculated the relative energies of ZIF-76-mbIm and TIF-4. However, DFT calculations on ZIFs with the formula $[Zn(Im)_2]$ have revealed that the LTA topology is higher in energy than the **cag** topology.[61,62] This implies that TIF-4, with the **cag** topology, is the more thermodynamically stable phase. Additionally, it has a much higher content of Im in its structure. Therefore, the addition of more Im immediately causes the formation of the more stable polymorph, TIF-4. Crystallographically, for the *Pbca* space group, asymmetric units with three or four bulky linkers have very low statistical frequencies (5%).[42] Additionally, mbIm cannot have an occupancy at any site of more than 0.5 to prevent collisions. Therefore, structures

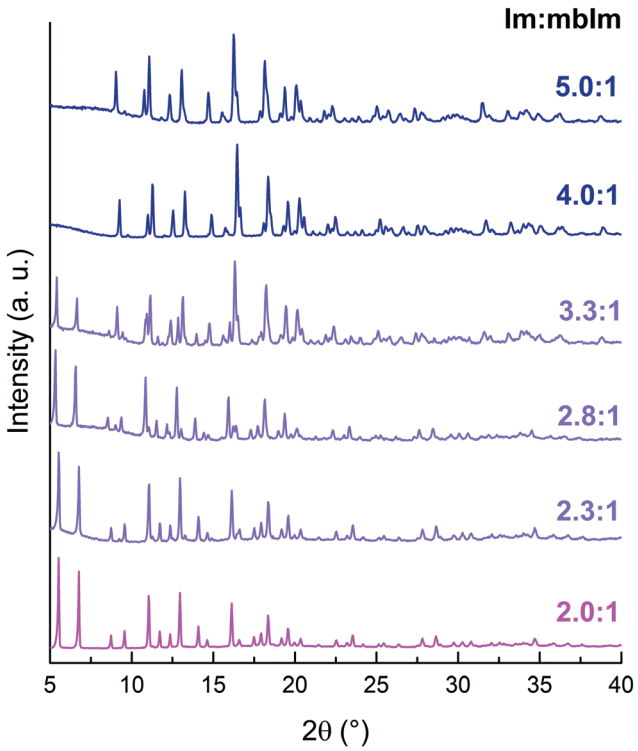

Fig. 5 Powder X-ray diffraction patterns of ZIF-76-mbIm. Systematically increasing the Im : mbIm ratio in the ZIF-76-mbIm synthesis from 2.0 : 1 to 5.0 : 1 gave sequentially pure ZIF-76-mbIm (pink), mixed phase ZIF-76-mbIm and TIF-4 (purple) then pure TIF-4 (dark blue).

with a formula with more mbIm than $[Zn(Im)_{1.5}(mbIm)_{0.5}]$ are inconsistent with the *Pbca* space group. Hence, to accommodate more bulky mbIm linker, the more porous cubic $P\bar{4}3m$ space group of ZIF-76-mbIm forms. Altering the linker ratio in the synthesis therefore gives subtle control over the resulting ZIF that forms.

Effect of framework topology on thermal behaviour

The thermal response of pure phase ZIF-76-mbIm [Zn(Im)(mbIm)] was measured (Fig. 6 and S37 and S38†). Fluctuations in the DSC trace in the range of 150–250 °C are ascribed to desolvation of residual solvent after activation. The presence of two peaks may be due to desolvation from different sized pores in the structure. ZIF-76-mbIm $[Zn(Im)_{1.33}(mbIm)_{0.67}]$ (mixed phase) is reported to melt at 471 °C with a decomposition temperature of 596 °C.[37] However, the DSC trace in this work for phase pure ZIF-76-mbIm [Zn(Im)(mbIm)] does not exhibit an endotherm in the expected temperature range. A very small endotherm with a lower offset of 409 °C was observed (Fig. 6 and S38†). This was followed by an exotherm accompanied with significant mass loss associated with sample decomposition.

A sequence of DSC heat treatments was performed in conjunction with ambient temperature powder X-ray diffraction in order to determine the origin of the

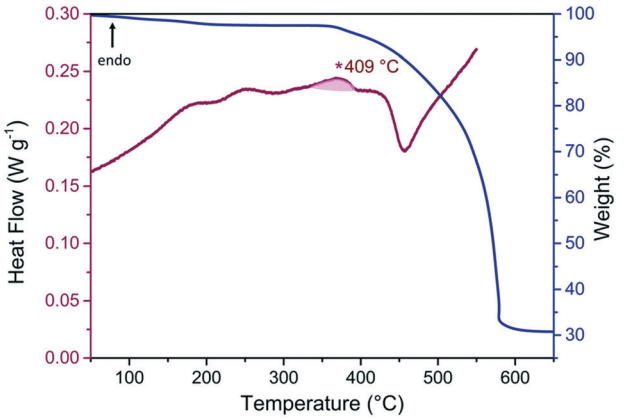

Fig. 6 TGA trace of ZIF-76-mbIm (blue) with significant mass loss occurring above 400 °C. DSC trace of ZIF-76-mbIm (pink) has an endothermic feature with an offset of 409 °C (marked by an asterisk and highlighted as a guide) followed by an exotherm associated with sample decomposition.

endotherm. Firstly, ZIF-76-mbIm was heated to 410 °C, *i.e.* beyond the offset of the endotherm, then cooled to room temperature (Fig. S39†). X-ray diffraction after heating revealed Bragg peaks, suggesting it was still crystalline (Fig. S40, Table S17†). Secondly, the sample was heated to 480 °C, *i.e.* within the exothermic region, then cooled to room temperature (Fig. S41†). X-ray diffraction again contained Bragg peaks assigned to the starting ZIF-76-mbIm framework (Fig. S42, Table S18†). ^{1}H NMR spectroscopy confirmed that the samples of ZIF-76-mbIm after heating to 410 °C and 480 °C had the same ratio of imidazolate to 5-methylbenzimidazolate as the parent material (Fig. S43 and S44†). Subsequently, these samples were re-heated in the DSC to 400 °C, *i.e.* above the glass transition temperature previously reported.[37] However, they did not exhibit features that might readily be linked to a glass transition.

To investigate this further, variable temperature total scattering data were collected (Fig. 7 and S45†). Total scattering data were collected at *ca.* 100 °C intervals to 400 °C, then at 430 °C, 450 °C and 460 °C. Measurements were also taken at room temperature before and after heating. Conversion to the corresponding $D(r)$ revealed that long-range order, *i.e.* atom–atom correlations exceeding 8 Å, reduced markedly after 400 °C (Fig. 7a). Significant changes were also observed in the short-range order region after 200 °C, *i.e.* for atom–atom correlations up to 8 Å. Comparison of a pristine sample of ZIF-76-mbIm and that returned to room temperature after heating to 460 °C showed marked differences (Fig. 7b) For example, the C=C/C–N correlation at 1.38 Å (1) shifts to 1.55 Å, *i.e.* close to that expected for a C–C single bond.[63] Im and mbIm are almost exclusively composed of aromatic C=C double bonds, so the formation of more C–C single bonds supports decomposition of the organic linkers or possible polymerisation. However, the sample changed colour in the X-ray beam from pale yellow to dark brown so decomposition may have been enhanced by beam damage. Furthermore, the Zn–N correlation peak at 2 Å

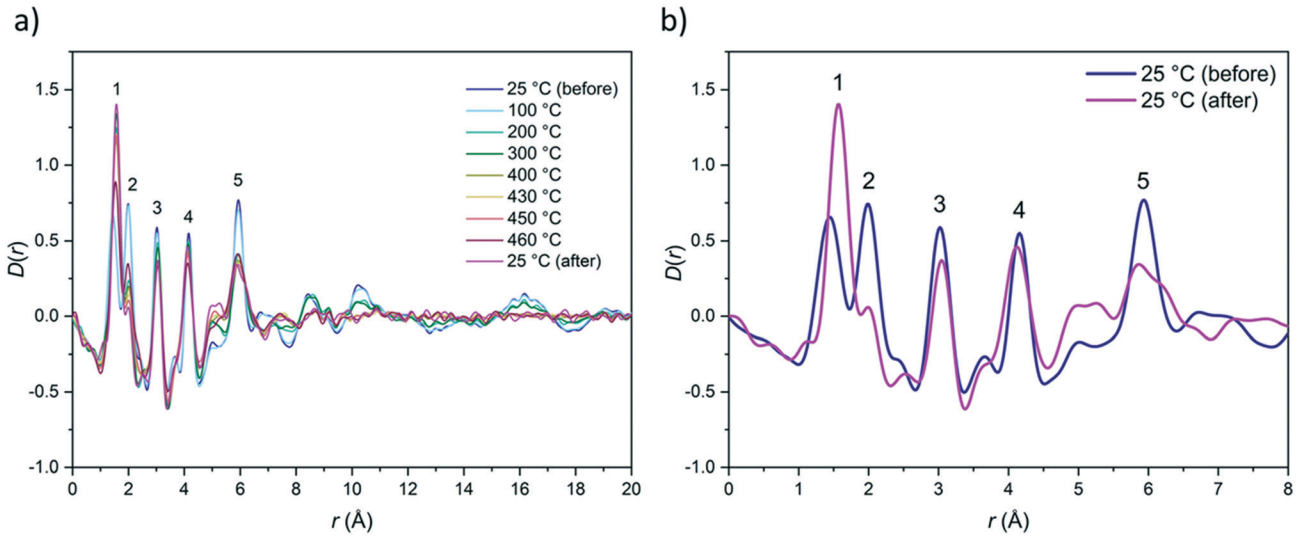

Fig. 7 Variable temperature PDF of ZIF-76-mbIm: a) long-range order is lost on heating above 400 °C; b) short-range order of ZIF-76-mbIm before and after heat treatment. The first five correlations are labelled (see Fig. 3 for imidazolate ion with these correlations labelled). Most notably, the C–C correlation (1) shifts to higher *r* and the Zn–N correlation (2) decreases. The same composition of [Zn(Im)(mbIm)] was used for the processing of all the data. However, it should be noted that as ZIF-76-mbIm had begun to decompose in the X-ray beam, it is unlikely that the sample composition would have remained constant throughout heating.

(2) decreases in intensity, which is unexpected given the retention of Zn–N bonding in other ZIF liquids and glasses.[23] Correlations (3) and (4), which are non-bonding interactions between Zn and C and N respectively, undergo minimal changes on heating. Finally, the Zn–Zn correlation (5) decreases in intensity and broadens significantly. This is accompanied by the growth of a broad correlation centred around 5.1 Å. These changes suggest that the local structure of the ZIF-76-mbIm framework evolves markedly on heating, hence supporting decomposition rather than melting.

To verify the original reports by Zhou *et al.* of ZIF-76-mbIm $[Zn(Im)_{1.33}(mbIm)_{0.67}]$ melting at 471 °C, a sample of ZIF-76-mbIm was synthesised using the reported procedure.[37] A mixed phase product (Fig. 4 and S15†) was prepared containing both ZIF-76-mbIm and TIF-4 with bulk composition $[Zn(Im)_{1.4}(mbIm)_{0.6}]$, confirmed by ^{1}H NMR (Fig. S46†). The thermal response of this sample was then investigated by DSC and TGA and confirmed the melting and decomposition features reported previously (Fig. S47 and S48†).[37] This means that samples of pure ZIF-76-mbIm, and samples containing a small amount of a dense polymorph impurity, behave differently upon heating. Longley *et al.* have reported the use of one high temperature MOF liquid, as a solvent for a secondary MOF component, which itself does not melt in the pure state under ambient pressure.[64] In the glass domain, the high temperature MOF liquid would be referred to as a flux.[64] They used ZIF-62 as a flux to induce melting in ZIF-8.[64] As discussed earlier, Gaillac *et al.* concluded that ZIF-8 does not melt on its own because of the high energy barrier to linker diffusion in its open network structure.[22,32,33]

These observations can rationalise both the results in this paper and those previously reported.[37] ZIF-76-mbIm, like ZIF-8, is a relatively porous, cubic framework. The barrier to linker dissociation therefore may be too high for melting to occur prior to sample decomposition. However, when TIF-4 is present as an impurity, it can assist the melting of ZIF-76-mbIm by acting as a flux. These results highlight the importance of crystal structure on melting and suggest the use of impure samples may be beneficial for glass formation, providing the impurity is a dense polymorph of the major product.

Effect of organic linker chemistry on ZIF-76

In a highly similar manner to ZIF-76-mbIm, the dense phase polymorph ZIF-UC-5 was also found to be an impurity in synthetic routines that aimed at producing ZIF-76 in high yields (Fig. S49, Table S19†).[37] In this previous work, ZIF-76 $[Zn(Im)_{1.62}(ClbIm)_{0.38}]$ was reported to melt at 451 °C.[37] The synthetic protocol which yielded pure phase ZIF-76-mbIm here was adapted to obtain phase pure ZIF-76 (Fig. S50, Table S20†). The chemical formula was found to be [Zn(Im)(ClbIm)] by ^{1}H NMR (Fig. S51†). Phase pure ZIF-76 [Zn(Im)(ClbIm)] was then analysed using DSC and TGA (Fig. 8 and S52 and S53†). It exhibited fluctuations in the DSC trace from 150–250 °C due to desolvation from residual solvent present in the pores. A small exotherm with an offset of 477 °C was present followed by a large second exotherm associated with mass loss and decomposition. Significant mass loss began above 450 °C suggesting that phase pure ZIF-76 has similar thermal stability to the sample reported previously.[37]

To investigate the nature of the first exotherm at 477 °C, a sequence of DSC heating treatments were performed along with room temperature powder X-ray diffraction. Firstly, ZIF-76 was heated to 410 °C, *i.e.* before the onset of the exotherm, then

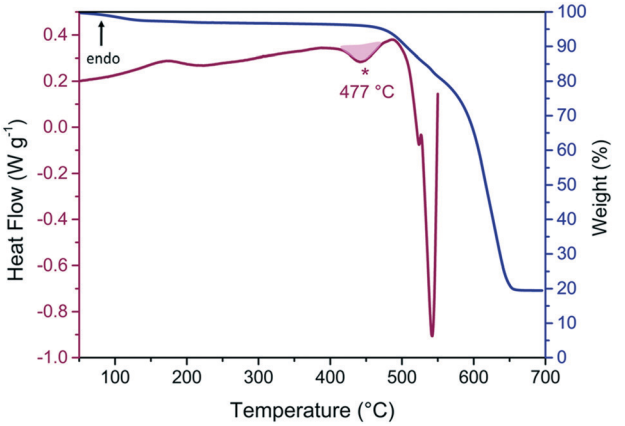

Fig. 8 TGA trace of ZIF-76 (blue) with significant mass loss occurring above 450 °C. DSC trace of ZIF-76 (pink) has an exothermic feature with an offset of 477 °C (marked by an asterisk and highlighted as a guide) followed by a larger exothermic feature associated with sample decomposition.

cooled to room temperature (Fig. S54†). Bragg peaks were visible in the X-ray diffraction pattern after heating, suggesting crystallinity was retained (Fig. S55, Table S21†). Secondly, ZIF-76 was heated to 480 °C, *i.e.* beyond the offset of the first exotherm but before the onset of the second larger exotherm, then cooled to room temperature (Fig. S56†). However, crystallinity was lost after heating ZIF-76 to 480 °C as the sample exhibited diffuse scattering in the X-ray diffraction pattern (Fig. S57†). ^{1}H NMR spectroscopy confirmed that after heating to 410 °C and 480 °C, ZIF-76 had the same ratio of imidazolate to 5-chlorobenzimidazolate as the parent material (Fig. S58 and S59†). Subsequently, these samples were re-heated in the DSC to 400 °C, *i.e.* above the glass transition temperature previously reported.[37] However, there were no discernible changes in the heat flow that may be consistent with a glass transition (Fig. S54 and S56†).

These results further show that the presence of a dense polymorph as an impurity is essential for porous glass formation. However, the thermal behaviour of ZIF-76 in the pure state is more complex than that of ZIF-76-mbIm. The major difference is that after heating to *ca.* 480 °C, the recovered sample of ZIF-76 is amorphous, whilst that of ZIF-76-mbIm remains crystalline. The amorphous sample of ZIF-76 does not however exhibit a glass transition. There are three possible explanations for this behaviour: (i) thermal solid-state amorphisation, which is observed in several other systems,[21] (ii) that the organic ligand decomposes, or (iii) the organic ligand undergoes a different structural change, *i.e.* rearrangement. The peak for the imidazole proton on 5-chlorobenzimidazole splits into multiple singlets on heating to 480 °C (Fig. S59†) so decomposition of the linker could be a viable explanation for the loss in crystallinity. Additionally, significant mass loss begins above 450 °C, which also supports sample decomposition. It is clear that subtle changes in linker chemistry have a strong influence over the thermal response of MOFs.

Conclusions

This work has used changes in linker chemistry and crystal structure to probe the resulting effects on MOF melting. It has also highlighted some promising strategies for reducing the melting temperature and glass transition temperature in ZIFs.

The control of linker chemistry over the thermal response of MOFs has been demonstrated. Changing the linker from mbIm to the more electron withdrawing ClbIm lowered the melting point from 440 °C to 428 °C and the T_g from 350 °C to 336 °C for the polymorphs TIF-4 and ZIF-UC-5. Additionally, changing the linker from mbIm to ClbIm caused ZIF-76 to exhibit diffuse X-ray scattering prior to decomposition. It was also found that increasing the ratio of Im : mbIm in TIF-4 from $[Zn(Im)_{1.5}(mbIm)_{0.5}]$ to $[Zn(Im)_{1.8}(mbIm)_{0.2}]$ caused a reduction in the melting temperature from 467 °C to 440 °C.[23,40]

The importance of the crystal structure of the parent crystalline MOF for melting has also been demonstrated. It has been found that melting and glass formation at ambient pressure do not occur in phase pure ZIF-76 [Zn(Im)(ClbIm)] or ZIF-76-mbIm [Zn(Im)(mbIm)], but can be induced by the presence of a dense polymorph in the product. This melts first, and then acts as a high temperature solvent for the remaining open pore polymorph.

In terms of potential for porosity, a_gTIF-4 and the crystalline phase of ZIF-UC-5 have been reported as effectively non-porous to N_2 gas, with BET surface areas of 0.49 m^2 g^{-1}, and 7.1 m^2 g^{-1} respectively.[23,43] Both glasses here are thus also anticipated to be dense in nature. ZIF-76 and ZIF-76-mbIm have however been reported to possess BET surface areas ranging between *ca.* 1200 and *ca.* 1600 m^2 g^{-1}, and micropore volumes of 0.60 μcm^3 g^{-1} and 0.58 μcm^3 g^{-1} respectively.[37,55] The retention of a portion of this porosity upon melting with a dense phase impurity leads to the ability to uptake CO_2.[37] These results are highly promising in suggesting that the rich polymorphic landscape in ZIFs may be taken advantage of to produce a range of flux-melted glasses arising from materials that do not melt in their phase pure form.

Conflicts of interest

There are no conflicts to declare.

Acknowledgements

A. M. B. acknowledges the Royal Society for funding (RGF\EA\180092) as well as the Cambridge Trust for a Vice Chancellor's Award (304253100). M. L. R. G. acknowledges project funding PAPIIT IG100618. M. F. T. would like to thank Corning Incorporated for PhD funding and project guidance. A. F. S. acknowledges the EPSRC for a PhD studentship under the industrial CASE scheme along with Johnson Matthey PLC (JM11106). L. L. acknowledges an EPSRC studentship. J. M. T. acknowledges funding from NanoDTC ESPSRC Grant EP/

L015978/1. T. D. B. thanks the Royal Society for both a University Research Fellowship (UF150021) and a research grant (RSG\R1\180395). T. D. B. also gratefully acknowledges the EPSRC (EP/R015481/1), and the University of Canterbury Te Whare Wānanga o Waitaha, New Zealand, for a University of Cambridge Visiting Canterbury Fellowship. We extend our gratitude to Diamond Light Source, Rutherford Appleton Laboratory, U.K., for access to beamline I15-1 (EE20038-2).

Notes and references

1 H. Li, M. Eddaoudi, M. O'Keeffe and O. M. Yaghi, *Nature*, 1999, **402**, 276–279.
2 B. F. Hoskins and R. Robson, *J. Am. Chem. Soc.*, 1989, **111**, 5962–5964.
3 S. Horike, S. Shimomura and S. Kitagawa, *Nat. Chem.*, 2009, **1**, 695–704.
4 H. Furukawa, K. E. Cordova, M. O'Keeffe and O. M. Yaghi, *Science*, 2013, **341**, 1230444.
5 A. J. Howarth, A. W. Peters, N. A. Vermeulen, T. C. Wang, J. T. Hupp and O. K. Farha, *Chem. Mater.*, 2017, **29**, 26–39.
6 M. Eddaoudi, D. B. Moler, H. Li, B. Chen, T. Reineke, M. O'Keeffe and O. M. Yaghi, *Acc. Chem. Res.*, 2001, **34**, 319–330.
7 I. Senkovska and S. Kaskel, *Chem. Commun.*, 2014, **50**, 7089–7098.
8 O. K. Farha, A. Ö. Yazaydin, I. Eryazici, C. D. Malliakas, B. G. Hauser, M. G. Kanatzidis, S. T. Nguyen, R. Q. Snurr and J. T. Hupp, *Nat. Chem.*, 2010, **2**, 944–948.
9 A. Dhakshinamoorthy, M. Alvaro, P. Horcajada, E. Gibson, M. Vishnuvarthan, A. Vimont, J. M. Grenèche, C. Serre, M. Daturi and H. Garcia, *ACS Catal.*, 2012, **2**, 2060–2065.
10 L. Mitchell, B. Gonzalez-Santiago, J. P. S. Mowat, M. E. Gunn, P. Williamson, N. Acerbi, M. L. Clarke and P. A. Wright, *Catal. Sci. Technol.*, 2013, **3**, 606–617.
11 P. Horcajada, R. Gref, T. Baati, P. K. Allan, G. Maurin, P. Couvreur, G. Férey, R. E. Morris and C. Serre, *Chem. Rev.*, 2012, **112**, 1232–1268.
12 A. J. Tansell, C. L. Jones and T. L. Easun, *Chem. Cent. J.*, 2017, **11**, 1–16.
13 P. Z. Moghadam, A. Li, S. B. Wiggin, A. Tao, A. G. P. Maloney, P. A. Wood, S. C. Ward and D. Fairen-Jimenez, *Chem. Mater.*, 2017, **29**, 2618–2625.
14 A. Schneemann, V. Bon, I. Schwedler, I. Senkovska, S. Kaskel and R. A. Fischer, *Chem. Soc. Rev.*, 2014, **43**, 6062–6096.
15 Z. Fang, B. Bueken, D. E. De Vos and R. A. Fischer, *Angew. Chem., Int. Ed.*, 2015, **54**, 7234–7254.
16 A. K. Cheetham, T. D. Bennett, F. X. Coudert and A. L. Goodwin, *Dalton Trans.*, 2016, **45**, 4113–4126.
17 T. D. Bennett and S. Horike, *Nat. Rev. Mater.*, 2018, **3**, 431–440.
18 S. C. McKellar and S. A. Moggach, *Acta Crystallogr., Sect. B: Struct. Sci., Cryst. Eng. Mater.*, 2015, **71**, 587–607.
19 K. W. Chapman, G. J. Halder and P. J. Chupas, *J. Am. Chem. Soc.*, 2009, **131**, 17546–17547.
20 T. D. Bennett, P. Simoncic, S. A. Moggach, F. Gozzo, P. MacChi, D. A. Keen, J.-C. Tan and A. K. Cheetham, *Chem. Commun.*, 2011, **47**, 7983–7985.
21 T. D. Bennett, D. A. Keen, J. C. Tan, E. R. Barney, A. L. Goodwin and A. K. Cheetham, *Angew. Chem., Int. Ed.*, 2011, **50**, 3067–3071.
22 R. Gaillac, P. Pullumbi, K. A. Beyer, K. Chapman, D. A. Keen, T. D. Bennett and F. X. Coudert, *Nat. Mater.*, 2017, **16**, 1149–1155.
23 T. D. Bennett, Y. Yue, P. Li, A. Qiao, H. Tao, N. G. Greaves, T. Richards, G. I. Lampronti, S. A. T. Redfern, F. Blanc, O. K. Farha, J. T. Hupp, A. K. Cheetham and D. A. Keen, *J. Am. Chem. Soc.*, 2016, **138**, 3484–3492.
24 D. Umeyama, N. P. Funnell, M. J. Cliffe, J. A. Hill, A. L. Goodwin, Y. Hijikata, T. Itakura, T. Okubo, S. Horike and S. Kitagawa, *Chem. Commun.*, 2015, **51**, 12728–12731.
25 D. Umeyama, S. Horike, M. Inukai, T. Itakura and S. Kitagawa, *J. Am. Chem. Soc.*, 2015, **137**, 864–870.
26 S. S. Nagarkar, H. Kurasho, N. T. T. Duong, Y. Nishiyama, S. Kitagawa and S. Horike, *Chem. Commun.*, 2019, **55**, 5455–5458.
27 E. T. Spielberg, E. Edengeiser, B. Mallick, M. Havenith and A. V. Mudring, *Chem. – Eur. J.*, 2014, **20**, 5338–5345.
28 Y. J. Su, Y. L. Cui, Y. Wang, R. B. Lin, W. X. Zhang, J. P. Zhang and X. M. Chen, *Cryst. Growth Des.*, 2015, **15**, 1735–1739.
29 K. S. Park, Z. Ni, A. P. Cote, J. Y. Choi, R. Huang, F. J. Uribe-Romo, H. K. Chae, M. O'Keeffe and O. M. Yaghi, *Proc. Natl. Acad. Sci. U. S. A.*, 2006, **103**, 10186–10191.
30 R. Banerjee, A. Phan, B. Wang, C. Knobler, H. Furukawa, M. O'Keeffe and O. M. Yaghi, *Science*, 2008, **319**, 939–943.
31 K. Noh, J. Lee and J. Kim, *Isr. J. Chem.*, 2018, **58**, 1075–1088.
32 R. Gaillac, P. Pullumbi and F. X. Coudert, *J. Phys. Chem. C*, 2018, **122**, 6730–6736.
33 T. D. Bennett, J. C. Tan, Y. Yue, E. Baxter, C. Ducati, N. J. Terrill, H. H. M. Yeung, Z. Zhou, W. Chen, S. Henke, A. K. Cheetham and G. N. Greaves, *Nat. Commun.*, 2015, **6**, 1–7.
34 L. Frentzel-Beyme, M. Kloß, R. Pallach, S. Salamon, H. Moldenhauer, J. Landers, H. Wende, J. Debus and S. Henke, *J. Mater. Chem. A*, 2019, **7**, 985–990.
35 L. Frentzel-Beyme, M. Kloß, P. Kolodzeiski, R. Pallach and S. Henke, *J. Am. Chem. Soc.*, 2019, **141**, 12362–12371.
36 Y. Zhao, S. Y. Lee, N. Becknell, O. M. Yaghi and C. A. Angell, *J. Am. Chem. Soc.*, 2016, **138**, 10818–10821.
37 C. Zhou, L. Longley, A. Krajnc, G. J. Smales, A. Qiao, I. Erucar, C. M. Doherty, A. W. Thornton, A. J. Hill, C. W. Ashling, O. T. Qazvini, S. J. Lee, P. A. Chater, N. J. Terrill, A. J. Smith, Y. Yue, G. Mali, D. A. Keen, S. G. Telfer and T. D. Bennett, *Nat. Commun.*, 2018, **9**, 5042.
38 T. D. Bennett, A. L. Goodwin, M. T. Dove, D. A. Keen, M. G. Tucker, E. R. Barney, A. K. Soper, E. G. Bithell, J. C. Tan and A. K. Cheetham, *Phys. Rev. Lett.*, 2010, **104**, 11503.
39 R. Lehnert and F. Seel, *Z. Anorg. Allg. Chem.*, 1980, **464**, 187–194.
40 T. Wu, X. Bu, J. Zhang and P. Feng, *Chem. Mater.*, 2008, **20**, 7377–7382.

41 J. B. James and Y. S. Lin, *J. Phys. Chem. C*, 2016, **120**, 14015–14026.
42 M. L. Ríos Gómez, G. I. Lampronti, Y. Yang, J. C. Mauro and T. D. Bennett, *Dalton Trans.*, 2020, **49**, 850–857.
43 J. Hou, M. L. Ríos Gómez, A. Krajnc, A. McCaul, S. Li, A. M. Bumstead, A. F. Sapnik, Z. Deng, R. Lin, P. A. Chater, D. S. Keeble, D. A. Keen, D. Appadoo, B. Chan, V. Chen, G. Mali and T. D. Bennett, *J. Am. Chem. Soc.*, 2020, **142**, 3880–3890.
44 L. Palatinus and G. Chapuis, *J. Appl. Crystallogr.*, 2007, **40**, 786–790.
45 G. M. Sheldrick, *Acta Crystallogr., Sect. C: Struct. Chem.*, 2015, **71**, 3–8.
46 L. J. Farrugia, *J. Appl. Crystallogr.*, 2012, **45**, 849–854.
47 R. N. Widmer, G. I. Lampronti, S. Anzellini, R. Gaillac, S. Farsang, C. Zhou, A. M. Belenguer, C. Wilson, H. Palmer, A. K. Kleppe, M. T. Wharmby, X. Yu, S. M. Cohen, S. G. Telfer, S. A. T. Redfern, F. X. Coudert, S. G. Macleod and T. D. Bennett, *Nat. Mater.*, 2019, **18**, 370–376.
48 R. N. Widmer, G. I. Lampronti, S. Chibani, C. W. Wilson, S. Anzellini, S. Farsang, A. K. Kleppe, N. P. M. Casati, S. G. Macleod, S. A. T. Redfern, F. X. Coudert and T. D. Bennett, *J. Am. Chem. Soc.*, 2019, **141**, 9330–9337.
49 S. Li, R. Limbach, L. Longley, A. Shirzadi, J. C. Walmsley, D. N. Johnstone, P. A. Midgley, L. Wondraczek and T. D. Bennett, *J. Am. Chem. Soc.*, 2019, **141**, 1027–1034.
50 A. Qiao, T. D. Bennett, H. Tao, A. Krajnc, G. Mali, C. M. Doherty, A. W. Thornton, J. C. Mauro, G. N. Greaves and Y. Yue, *Sci. Adv.*, 2018, **4**, 1–7.
51 A. A. Coelho, *TOPAS-Academic (Version 6)*, Coelho Software, Brisbane, 2016.
52 Bruker, *TopSpin (Version 4.0.7)*, Bruker, Billerica, MA, 2019.
53 A. K. Soper and E. R. Barney, *J. Appl. Crystallogr.*, 2011, **44**, 714–726.
54 A. K. Soper, *Sci. Technol. Facil. Counc. Tech. Rep. RAL-TR-2011-013*, 2011, pp. 1–135.
55 D. Peralta, G. Chaplais, A. Simon-Masseron, K. Barthelet and G. D. Pirngruber, *Microporous Mesoporous Mater.*, 2012, **153**, 1–7.
56 A. Bondi, *J. Phys. Chem.*, 1964, **68**, 441–451.
57 J. Yang, Y. B. Zhang, Q. Liu, C. A. Trickett, E. Gutiérrez-Puebla, M. Á. Monge, H. Cong, A. Aldossary, H. Deng and O. M. Yaghi, *J. Am. Chem. Soc.*, 2017, **139**, 6448–6455.
58 J. M. Tuffnell, C. W. Ashling, J. Hou, S. Li, L. Longley, M. L. Rios Gomez and T. D. Bennett, *Chem. Commun.*, 2019, **55**, 8705–8715.
59 C. Zhou, M. Stepniewska, L. Longley, C. W. Ashling, P. A. Chater, D. A. Keen, T. D. Bennett and Y. Yue, *Phys. Chem. Chem. Phys.*, 2018, **20**, 18291–18296.
60 J. Catalán, R. M. Claramunt, J. Elguero, J. Laynez, M. Menéndez, F. Anvia, J. H. Quian, M. Taagepera and R. W. Taft, *J. Am. Chem. Soc.*, 1988, **110**, 4105–4111.
61 D. W. Lewis, A. R. Ruiz-Salvador, A. Gómez, L. M. Rodriguez-Albelo, F.-X. Coudert, B. Slater, A. K. Cheetham and C. Mellot-Draznieks, *CrystEngComm*, 2009, **11**, 2272.
62 C. Mellot-Draznieks and B. Kerkeni, *Mol. Simul.*, 2014, **40**, 25–32.
63 L. S. Bartell, *J. Am. Chem. Soc.*, 1959, **81**, 3497–3498.
64 L. Longley, S. M. Collins, G. J. Smales, I. Erucar, A. Qiao, J. Hou, C. M. Doherty, A. Thornton, A. J. Hill, X. Yu, N. J. Terrill, A. J. Smith, S. M. Cohen, P. A. Midgley, D. A. Keen, S. G. Telfer and T. D. Bennett, *Chem. Sci.*, 2019, **10**, 3592–3601.